pISSN 2384-1095
eISSN 2384-1109

iMRI 2019;23:114-124

https://doi.org/10.13104/imri.2019.23.2.114

iMRI
Investigative Magnetic Resonance Imaging

Biases in the Assessment of Left Ventricular Function by Compressed Sensing Cardiovascular Cine MRI

Jong-Hyun Yoon[1], Pan-ki Kim[2], Young-Joong Yang[1], Jinho Park[3], Byoung Wook Choi[2], Chang-Beom Ahn[1]

[1]Department of Electrical Engineering, Kwangwoon University, Seoul, Korea
[2]Department of Radiology, Severance Hospital, Yonsei University, Seoul, Korea
[3]Developing Brain Research Laboratory, Children's National Health System, Washington, DC, USA

Original Article

Received: February 8, 2019
Revised: March 25, 2019
Accepted: April 16, 2019

Correspondence to:
Chang-Beom Ahn, Ph.D.
Department of Electrical Engineering, Kwangwoon University, 20 Kwangwoon-ro, Nowon-gu, Seoul 01897, Korea
Tel. +82-2-940-5148
Fax. +82-2-909-3159
E-mail: cbahn@kw.ac.kr

This is an Open Access article distributed under the terms of the Creative Commons Attribution Non-Commercial License (http://creativecommons.org/licenses/by-nc/4.0/) which permits unrestricted non-commercial use, distribution, and reproduction in any medium, provided the original work is properly cited.

Copyright © 2019 Korean Society of Magnetic Resonance in Medicine (KSMRM)

Purpose: We investigate biases in the assessments of left ventricular function (LVF), by compressed sensing (CS)-cine magnetic resonance imaging (MRI).
Materials and Methods: Cardiovascular cine images with short axis view, were obtained for 8 volunteers without CS. LVFs were assessed with subsampled data, with compression factors (CF) of 2, 3, 4, and 8. A semi-automatic segmentation program was used, for the assessment. The assessments by 3 CS methods (ITSC, FOCUSS, and view sharing (VS)), were compared to those without CS. Bland-Altman analysis and paired t-test were used, for comparison. In addition, real-time CS-cine imaging was also performed, with CF of 2, 3, 4, and 8 for the same volunteers. Assessments of LVF were similarly made, for CS data. A fixed compensation technique is suggested, to reduce the bias.
Results: The assessment of LVF by CS-cine, includes bias and random noise. Bias appeared much larger than random noise. Median of end-diastolic volume (EDV) with CS-cine (ITSC or FOCUSS) appeared -1.4% to -7.1% smaller, compared to that of standard cine, depending on CF from (2 to 8). End-systolic volume (ESV) appeared +1.6% to +14.3% larger, stroke volume (SV), -2.4% to -16.4% smaller, and ejection fraction (EF), -1.1% to -9.2% smaller, with $P < 0.05$. Bias was reduced from -5.6% to -1.8% for EF, by compensation applied to real-time CS-cine (CF = 8).
Conclusion: Loss of temporal resolution by adopting missing data from nearby cardiac frames, causes an underestimation for EDV, and an overestimation for ESV, resulting in underestimations for SV and EF. The bias is not random. Thus it should be removed or reduced for better diagnosis. A fixed compensation is suggested, to reduce bias in the assessment of LVF.

Keywords: Cardiovascular cine MRI; Left ventricular function; Compressed sensing; Bias; Compensation

INTRODUCTION

Cardiovascular cine MRI has been recognized, as an accurate noninvasive method for assessing left ventricular function (1, 2). For cardiovascular cine MRI, CS is a useful technique to reduce scan time, thereby keeping high temporal and spatial resolutions, without high-end hardware (3-6). The CS technique has often been combined with

parallel imaging, to reduce scan time further (7-11). Since cardiac cine MRI data are acquired in k-t space, spatial and temporal resolutions are interrelated. Performance of the CS method is often evaluated with undersampled data, once full data is acquired, and normalized mean square error (NMSE) of the reconstructed images is evaluated, as a function of CF with respect to reference images without CS (12).

Assessment of LVF using cardiovascular cine MRI (termed as "standard cine"), has been widely used for clinical applications (13-16). EDV, ESV, SV, mass, and EF are often used as the LVF parameters (17-20). Influence of spatial and temporal resolutions on LVF parameters in standard cine MRI, was reported (21). Cardiovascular cine MRI with CS (termed as "CS-cine"), has also been used for clinical applications (22-25). Biases were observed in assessment of LVF by CS-cine in several reports (23, 24, 26); however, they were often attributed to experimental errors due to cardiac and respiratory motions, or inaccurate segmentation of blood volume (26, 27). In this paper, we investigate bias, separately from other experimental or physiological errors. Bias is different from random noise. It could be reduced by proper compensation.

MATERIALS AND METHODS

There are several sources of error in the assessment of LVF by cardiovascular cine MRI. Inaccurate localization of selection planes due to cardiac and respiratory motions, is one of the error sources. Inconsistent segmentation of the ventricular volume is another error source. The CS-cine introduces additional error due to sparse sampling, resulting in loss of spatial and temporal resolution. To separate the error by CS-cine from other sources, we generated undersampled data sets, from fully acquired data set retrospectively, thereby excluding errors due to cardiac and respiratory motion. An automatic segmentation program was developed, to ensure consistent segmentation.

Eight healthy volunteers (7 male and 1 female, age = 24.9 ± 2.23, BMI = 22.0 ± 1.77 kg/m^2) participated in the experiments. Standard cine MRI data with a short axis view, were acquired from a 3.0T MRI system (Siemens, Magnetom Trio, Erlangen, Germany). A segmented cine imaging (28) with a balanced steady state free precession (SSFP) sequence (29), was used with parameters: repetition time (TR) = 3.88 ms, echo time = 1.94 ms, views per segment (VPS) = 8, flip angle = 47°, transverse resolution = 1.37 mm × 1.37 mm, slice thickness = 8 mm, field-of-view = 350 mm × 350 mm, and number of slices = 12. A sensitivity encoding (SENSE) factor of 2 was used, throughout the experiments. The data set acquired without CS, were defined as 'fully acquired data set'. From the fully acquired data set, 4 undersampled data sets were generated with CF = 2, 3, 4, and 8. In addition, CS-cine imaging to acquire undersampled data directly, was also conducted. We referred to 'real-time CS-cine' to emphasize direct undersampling, in contrast to retrospective undersampling after full acquisition. Progressive ECG gating was used, for measurements with a breath-hold. All the studies were approved by the Institutional Review Board. Written informed consents were obtained, from all participating volunteers.

Three CS methods were used for comparison: FOCal Underdetermined System Solver (FOCUSS) (30), Iterative Truncation of Small transformed Coefficients (ITSC) (12), and view sharing (VS) (31). VS may not be considered as CS; however it was included, as a simple example of sparse sampling. Each CS method used its own sampling strategy, e.g., FOCUSS and ITSC used random sampling, with given probability density functions, while VS used periodic sampling with one sampling shifted for each cardiac frame. Only even phase encoding locations were used for all the methods, to combine CS with parallel imaging (SENSE factor = 2). Once reconstruction for CS is done, folded images are obtained, which are unfolded by SENSE reconstruction in separation, to CS for all the methods, as shown in Figure 1 (12).

We used a home-built automatic program, to segment the left ventricular volume. Only two seed points are required, to segment entire multi-slice cardiac cine images; one at the inside left ventricle, and the other at the myocardium. Then the seed points automatically change their locations, depending on cardiac phase and slice position. The program starts with a threshold set by the middle value of the means of the pixels, around seed points. After segmentation of the left ventricle and myocardium by the threshold, the threshold is updated by the middle value of the means of the segmented pixels, of the ventricle and myocardium. A refined segmentation is then performed, using the updated threshold. Since most of the pixels in the myocardium and the ventricle are involved to update the threshold, initial seed locations are not critical to segmentation. The segmentation method is applied for all the cardiac slices, irrespective of CS method and CF.

The assessment of LVF by cine without CS (CF = 1) was

chosen as the ground truth. Normalized difference (ND) is defined as the difference of the assessments by CS-cine and CS-standard (reference) divided by that of CS-standard, given by

$$ND_Q = \frac{Q_{CS} - Q_{ref}}{Q_{ref}} \times 100\ [\%] \quad [1],$$

where Q represents EDV, ESV, SV, and EF. Mass was excluded in this study due to the difficulties in defining epicardium of the left ventricle by the segmentation program. The normalization reduces personal variations of the quantities. Bias is defined by the mean of NDs. Effect of random sampling for CS may appear random noise on ND. The random noise is relatively small if CF is not too high, thus is not considered in this analysis.

Since the bias has a fixed polarity, it can be compensated. If we introduce a compensation factor α such that

$$Q_C = Q/(1+\alpha) \quad [2]$$

where, Q_C is compensated value from the initial assessment, Q by CS-cine. The factor is to compensate for the amount of underestimation or overestimation. Note that the factor α is similar to ND in Eq. [1], thus α may be chosen as the mean of NDs, by which the average bias can be removed. Once the EDV and ESV are compensated, then SV and EF will subsequently be compensated by definition.

RESULTS

Figure 2 shows NDs for EDV and ESV for 8 volunteers for three CS methods as a function of CF. Volunteers are represented by different marks and colors. Mean and median values of ND for 8 volunteers are shown in broken and solid lines, respectively. Figure 2 shows that as CF increases, mean and median values of NDs for EDV decrease, while those of ESV increase. Larger NDs are observed for VS, compared to those for FOCUSS and ITSC. Figure 3 shows that mean and median values of NDs for SV decrease, as CF increases. Since SV is defined by EDV-ESV, SV decreases more rapidly as CF increases. The EF defined by SV/EDV decreases as CF increases, since SV decreases more rapidly than EDV. The trends (decreases of EDV, SV, and EF, and an increase of ESV) are consistent, regardless of CS method.

Table 1 summarizes the median, mean, and standard deviation (SD) of NDs for 8 volunteers. Table 1 shows means of NDs for ITSC and FOCUSS varied -1.3% to -8.7% for EDV, +1.8% to +16.3% for ESV, -2.3% to -17.4% for SV, and -1.0% to -9.6% for EF for the change of CF from 2 to 8. The means of NDs for VS had much larger variations. In most of the cases medians of NDs were slightly lower than means. P-value, the probability that has no systematic bias between CS-cine and standard cine, appeared less than 5%. Thus, no systematic bias is hardly acceptable.

Figure 4 shows Bland-Altman plots for LVFs assessed by CS-cine (FOCUSS with CF = 4) and standard cine. Mean of

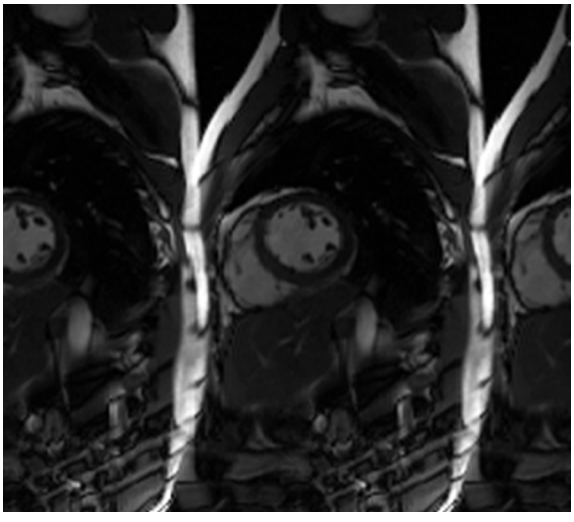

a

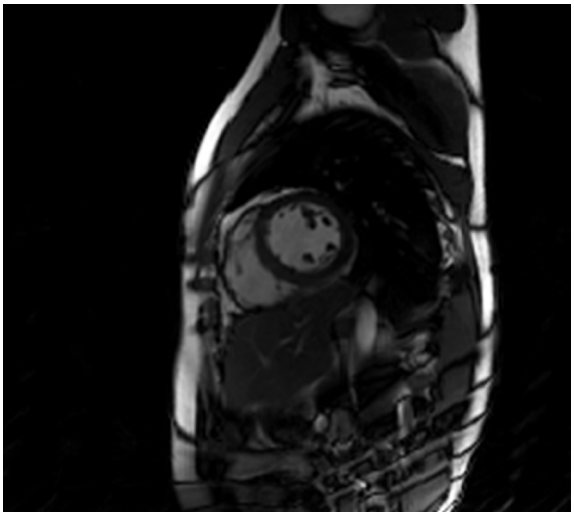

b

Fig. 1. Reconstructions for CS and parallel imaging, are performed sequentially. First, (a) reconstruction for CS is performed, and folded image is obtained, and then (b) SENSE reconstruction is applied to the folded image, to obtain unfolded image. Only even phase encoding locations are used.

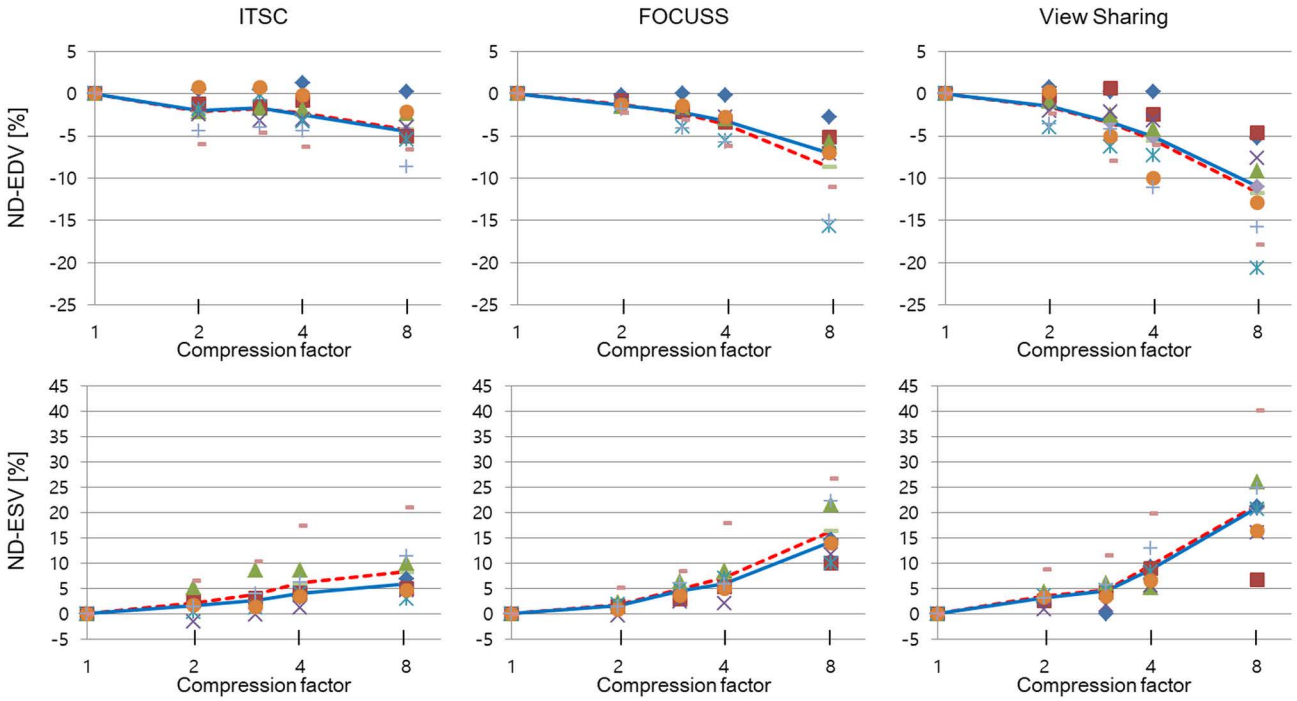

Fig. 2. Normalized differences for EDV and ESV for 8 volunteers are depicted, as a function of CF for 3 CS methods. Mean and median of the normalized differences, are shown in broken and solid lines, respectively.

Table 1. The Median, Mean, SD, and P Values of the Normalized Differences of LVF for 8 Volunteers are Summarized for 3 CS-cine Methods

LVF	CS method	CF = 2				CF = 3				CF = 4				CF = 8			
		median	mean	SD	P	median	mean	SD	P	median	mean	SD	P	median	mean	SD	P
EDV	ITSC	-1.97	-2.12	2.27	3.50	-1.67	-1.78	2.05	4.63	-2.47	-2.33	2.44	3.25	-4.52	-4.25	2.82	0.59
	FOCUSS	-1.38	-1.26	0.66	0.11	-2.21	-2.33	1.37	0.24	-3.19	-3.68	2.01	0.12	-7.06	-8.71	4.75	0.13
	VS	-1.48	-1.54	1.76	4.76	-3.39	-3.42	3.02	1.14	-5.14	-5.52	3.87	0.80	-11.01	-11.72	6.00	0.05
ESV	ITSC	1.60	2.20	2.60	4.88	2.72	3.84	3.70	1.76	4.08	6.07	5.08	0.10	5.93	8.29	5.91	0.03
	FOCUSS	1.65	1.81	1.54	0.27	4.55	4.87	2.03	0.01	5.86	7.18	4.69	0.01	14.28	16.34	6.28	0.01
	VS	3.14	3.60	2.33	0.01	4.49	4.68	3.48	0.15	8.66	9.57	4.86	0.00	20.90	21.49	9.66	0.01
SV	ITSC	-3.02	-3.46	2.91	1.63	-4.20	-3.60	2.97	1.38	-5.55	-4.93	3.34	0.57	-8.18	-8.35	3.37	0.09
	FOCUSS	-2.39	-2.28	0.89	0.03	-4.88	-4.82	1.62	0.01	-7.93	-7.32	2.51	0.01	-16.39	-17.43	4.97	0.01
	VS	-3.30	-3.22	2.27	0.57	-6.52	-5.92	4.16	0.46	-9.45	-10.58	4.38	0.10	-24.08	-23.14	7.64	0.01
EF	ITSC	-1.15	-1.38	1.07	0.82	-1.67	-1.86	1.44	0.77	-2.56	-2.68	1.32	0.11	-4.47	-4.30	1.17	0.00
	FOCUSS	-1.09	-1.03	0.43	0.03	-2.41	-2.56	0.67	0.00	-3.80	-3.79	1.15	0.00	-9.18	-9.57	1.98	0.00
	VS	-1.55	-1.71	0.71	0.03	-2.85	-2.62	1.50	0.18	-5.35	-5.38	1.05	0.00	-11.94	-13.05	4.20	0.00

All the units are in percentage.

CF = compression factor; CS = compressed sensing; EDV = end-diastolic volume; EF = ejection fraction; ESV = end-systolic volume; FOCUSS = FOCal Underdetermined System Solver; LVF = left ventricular function; ITSC = Iterative Truncation of Small transformed Coefficients; SD = standard deviation; SV = stroke volume; VS = view sharing

difference (denoted as 'Mean') and range of 95% confidence interval of the mean difference (CIMD), are shown in blue solid and dashed lines, respectively. The 95% confidence interval of the difference (CID), is also shown in dark-brown dotted lines (denoted as '+/- 1.96 SD'). The SD is due to personal variations of LVFs. P-value is shown in parenthesis next to mean of difference. If $P < 0.05$, there is a high possibility of systematic bias. The Student's t-distribution is used for evaluating CIMD and P-value, since the number of volunteers is not large. The Bland-Altman analysis reveals that mean differences between CS-cine and the standard cine are -3.2 ml for EDV (95% CID, -6.5 ml to 0.2 ml), 1.5 ml for ESV (95% CID, 0.4 ml to 2.6 ml), -4.7 ml for SV (95% CID, -8.0 ml to -1.4 ml, and -2.8% for EF (95% CID, -4.4% to -1.1%). Figure 4 confirms that significant biases exist, between CS-cine and standard cine for all EDV, ESV, SV, and EF, with $P < 0.005$.

Retrospective undersampling after full acquisition of cine data, may not be practical for clinical applications. Bland-Altman plots for real-time CS-cine and standard cine, are shown in Figure 5. For real-time CS-cine, 8 slices, per breath-hold are acquired (CF = 8) directly by ITSC. Mean differences appeared larger compared to those in Figure 4, due to larger CF. Larger SD, thereby larger CID and CIMD are found in Figure 5, since real-time CS-cine is measured separately, not undersampled from the data of standard cine. Thus, experimental variations are involved. Figure 5 shows that significant biases exist, between real-time CS-cine and standard cine ($P < 0.02$), implying that the biases are larger, than the experimental variations for the case of CF = 8. The Bland-Altman analysis in Figure 5 shows that the mean differences between real-time CS-cine (CF = 8) and standard cine, are -6.0 ml for EDV (95% CID, -16.9 ml to 5.0 ml), 3.1 ml for ESV (95% CID, -1.3 ml to 7.6 ml), -9.1 ml for SV (95% CID, -19.5 ml to 1.3 ml), and -5.6% for EF (95% CID, -10.1% to -1.2%).

Bland-Altman plots shown in Figure 4, are redrawn in Figure 6, with compensation. Mean differences change to 0.1 ml for EDV (95% CID, -3.7 ml to 3.8 ml), -0.2 ml for ESV (95% CID, -1.6 ml to 1.2 ml), 0.3 ml for SV (95% CID, -4.3 ml to 4.9 ml), and 0.3% for EF (95% CID, -2.1% to 2.6%). Note that biases shown in Figure 4, almost disappear in Figure 6 with $P > 0.46$. Similarly, Bland-Altman plots shown in Figure 5, are redrawn in Figure 7 with compensation. Mean differences appear -2.3 ml for EDV (95% CID, -13.5 ml to 9.0 ml), 1.1 ml for ESV (95% CID, -3.2 ml to 5.3 ml), -3.3 ml for SV (95% CID, -14.4 ml to 7.8 ml), and -1.8% for EF (95% CID, -6.8% to 3.1%). Figure 7 also shows the

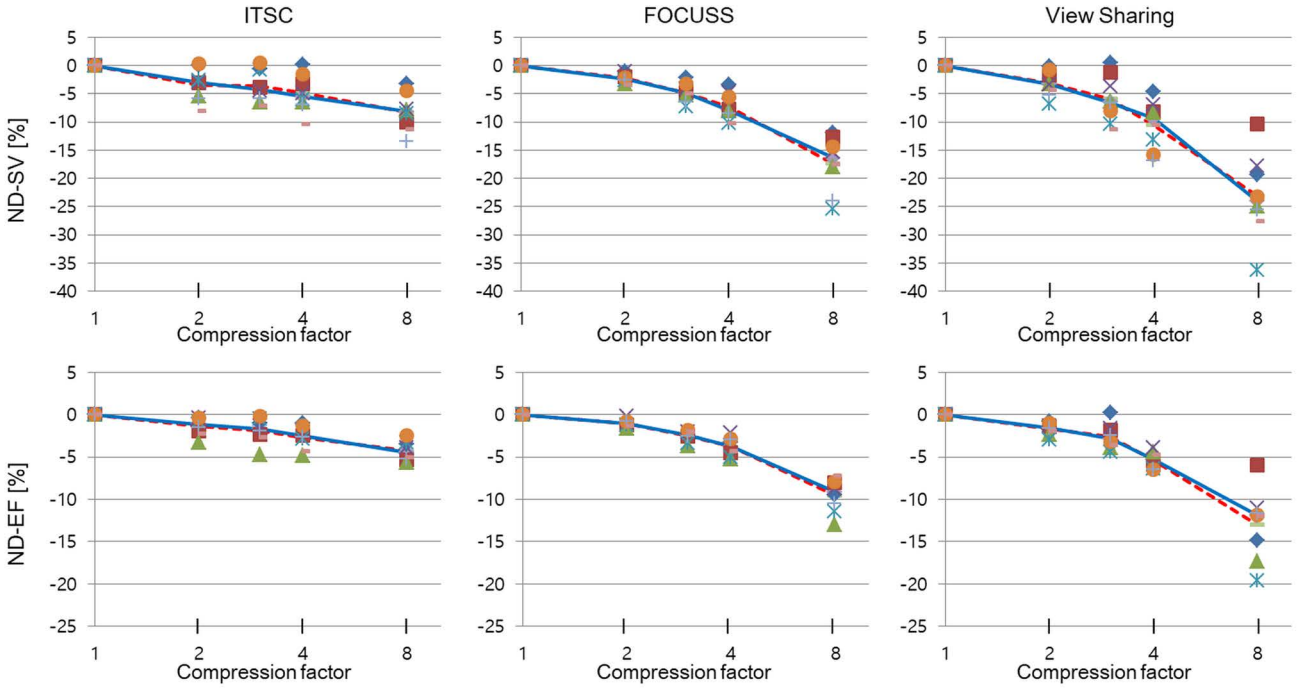

Fig. 3. Normalized differences for SV and EF for 8 volunteers are shown, as a function of CF for 3 CS methods. Mean and median are shown in broken and solid lines.

biases are substantially reduced (0.1 < P < 0.3), although compensation is not as perfect as the previous case shown in Figure 6, due to the experimental error involved.

DISCUSSION

Compressed sensing (CS) has been widely used for cardiovascular cine MRI, due to high temporal correlation in cine images and easy implementation on existing MRI system, without additional high-performance hardware. Most studies have concluded that CS-cine, is as good as standard cine for diagnosis. However, small differences were observed between assessments, by standard cine and CS-cine in some reports. Such differences were not fully investigated, since they were mixed with experimental variations, due to cardiac and respiratory motions, and subjective segmentation.

Three CS methods (FOCUSS, ITSC, and VS) were used, for assessment of LVF. The FOCUSS iteratively finds a solution (reconstruction) by the weighted L2-norm minimization, by assigning the currently reconstructed image, as the weight matrix for the next iteration, by which minimization of L1-norm is achieved. The ITSC tries L1-norm minimization

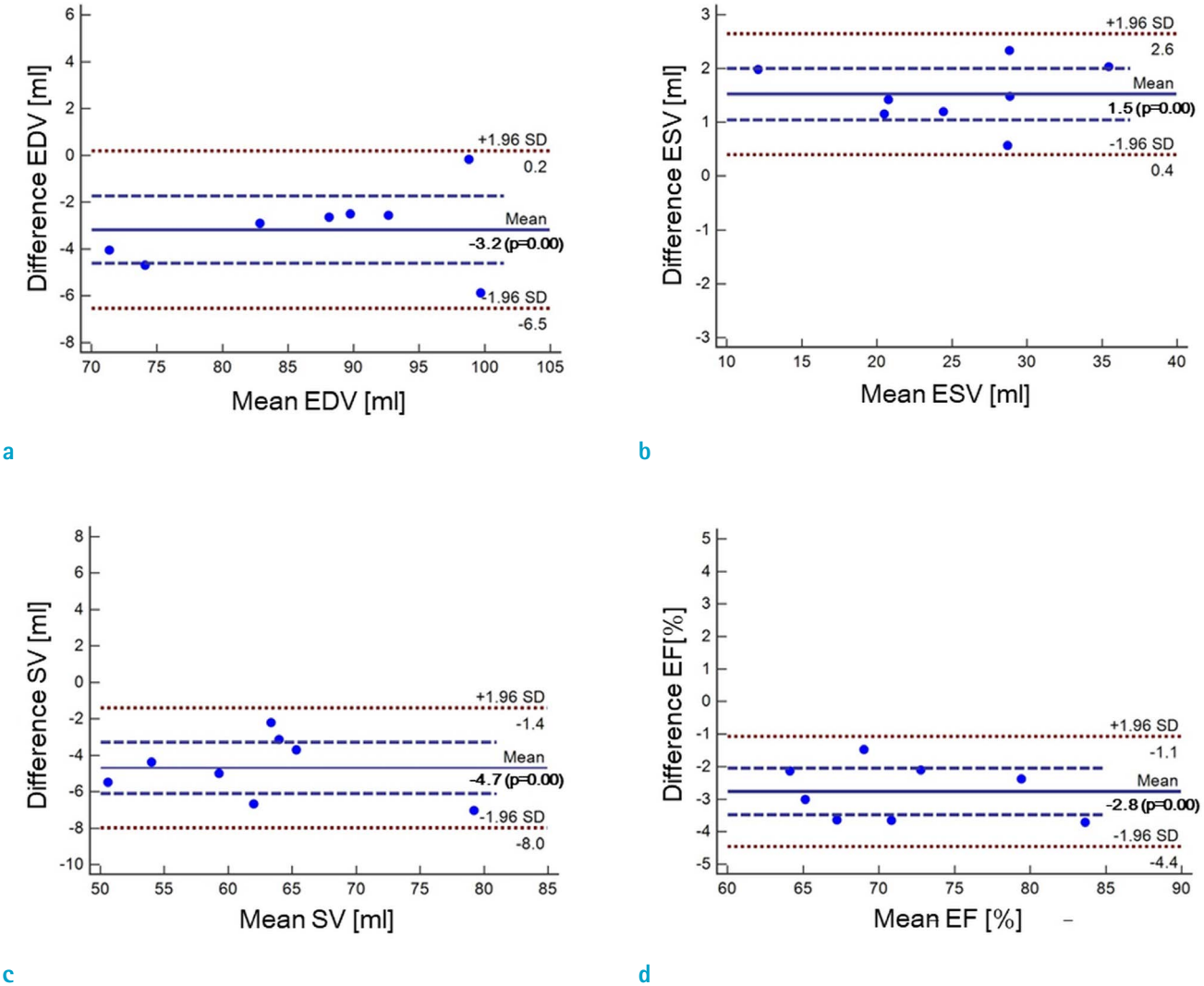

Fig. 4. Bland-Altman plots for assessments of LVF by CS-cine (FOCUSS, CF = 4) and standard cine: (a) EDV, (b) ESV, (c) SV, and (d) EF. Mean of difference ('Mean') and range of 95% confidence interval of the mean difference (CIMD), are shown in blue solid and dashed lines. The 95% confidence interval of the difference (CID), is also shown in dark-brown dotted lines. P-value is shown next to the mean of difference. Significant biases (P < 0.005) are found for all EDV, ESV, SV, and EF.

by truncating small coefficients in a transformed space, yet restoring measured data in k-space iteratively, until reconstructed images converge. VS shares data at nearby cardiac frames in k-space, with conventional Fourier transform for reconstruction.

In cardiac cycle, EDV (or ESV) is assessed at the phase when blood volume reaches a maximum (or a minimum). Practically, a time duration (e.g., VPS × TR [s] for the segmented cine MRI) rather than an instance, is allowed to form a cardiac frame, to reduce scan time. Thus, an average volume for duration, is assessed for EDV or ESV effectively. For CS-cine, the time duration is further extended, by adopting missing data at nearby cardiac frames. Extended time duration attenuates peaks for EDV and ESV, due to time average effects. The SV that is given by (EDV - ESV) would be further reduced. The EF that is given by (SV/EDV) would also be reduced. Thus, loss of temporal resolution results in negative biases for EDV, SV, and EF, and a positive bias for ESV as shown in Figures 2 and 3. As CF increases, amounts of bias increase, due to lengthier time average effects. Since the biases for EDV and ESV have opposite polarities, they cannot be considered results of blurring or filtering.

As to the total number of subjects (= 8), it may be marginal. However, it was not easy to measure cine data for various CFs. For example, 12 breath-holds were needed for the acquisition of 12 slices without compression (CF = 1), 6 breath-holds for the real-time CS-cine with CF = 2,

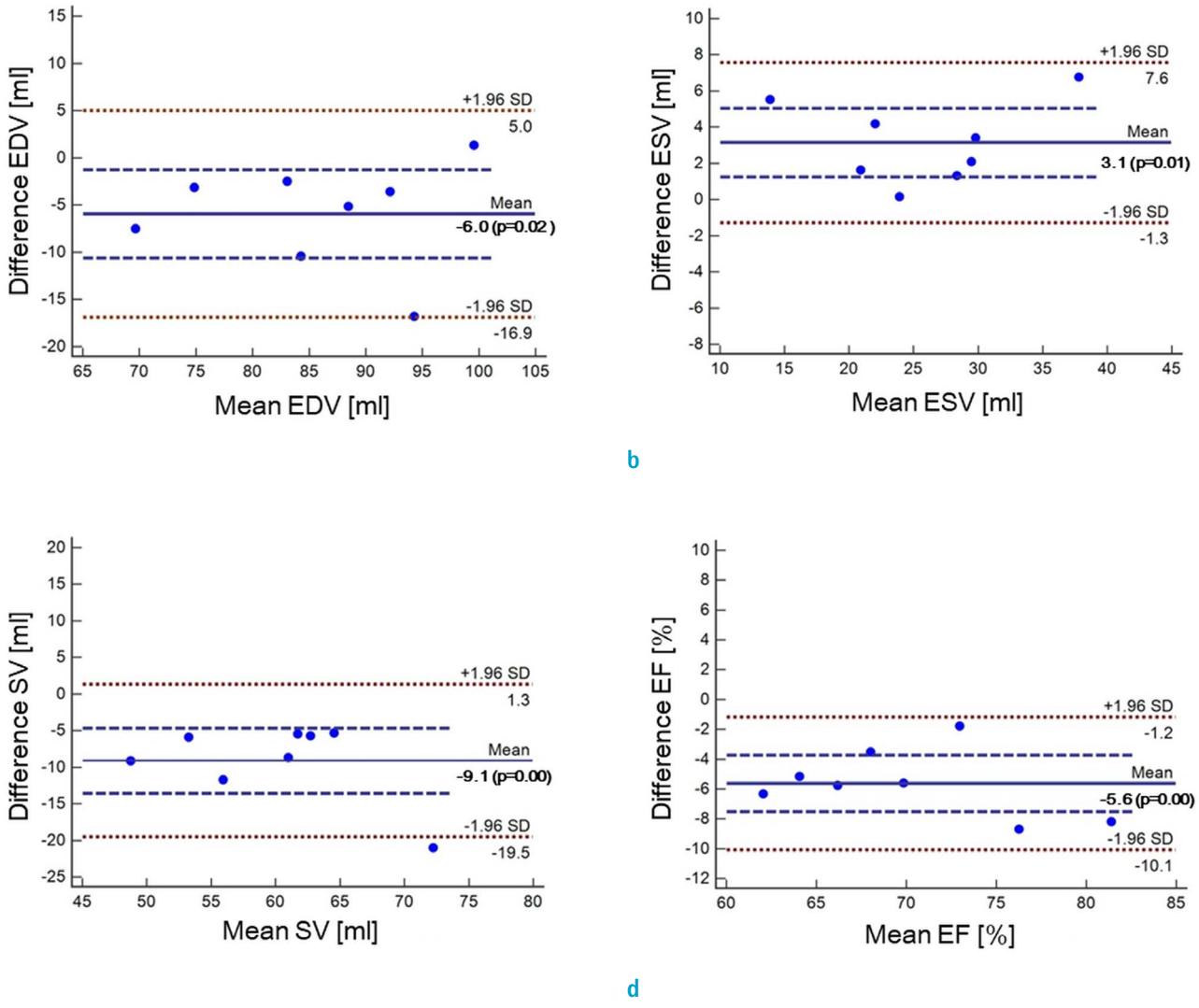

Fig. 5. Bland-Altman plots for assessments of LVF by real time CS-cine (ITSC, CF = 8) and standard cine: (a) EDV, (b) ESV, (c) SV, and (d) EF. Significant biases are found for all EDV, ESV, SV, and EF ($P < 0.02$).

4 breath-holds for CF = 3, 3 breath-holds for CF = 4, and 2 breath-holds for CF = 8. Thus, a total of 27 breath-holds were needed, for the study for each volunteer. Since the biases appeared consistent (negative biases for EDV, SV, and EF, and positive bias for ESV, and larger biases with higher CF) for all the volunteers, it could be concluded, that the biases are due to loss of temporal resolution by CS-cine. The biases were also consistent with previous publications (23, 24, 26).

Biases are clearly seen in Figure 4 and 5, with Bland-Altman plots. For example zero points (null bias) are far out CIMD for EDV, ESV, SV, and EF in Figures 4 and 5. Differences between assessments by CS-cine and standard cine, appeared as large as -2.8% to -5.6% for EF with CF from 4 to 8. Such bias could influence diagnosis. For example, approximately 10% variation of EF, could shift diagnostic categories, from "mildly abnormal" to "moderately abnormal" to "severely abnormal" (32, 33). Thus, the bias should not be ignored.

Since the bias has a fixed polarity and magnitude, it can be reduced by proper compensation. We proposed a fixed compensation model for given CS and CF, equivalent to moving the bias by a fixed amount. Choosing the compensation factor as the mean of NDs, the bias is reduced substantially, as shown in Figure 6. In real-time CS-cine, compensation may not be achieved perfectly, since there are experimental and physiological variations. Figure 7 shows that the compensation works properly even

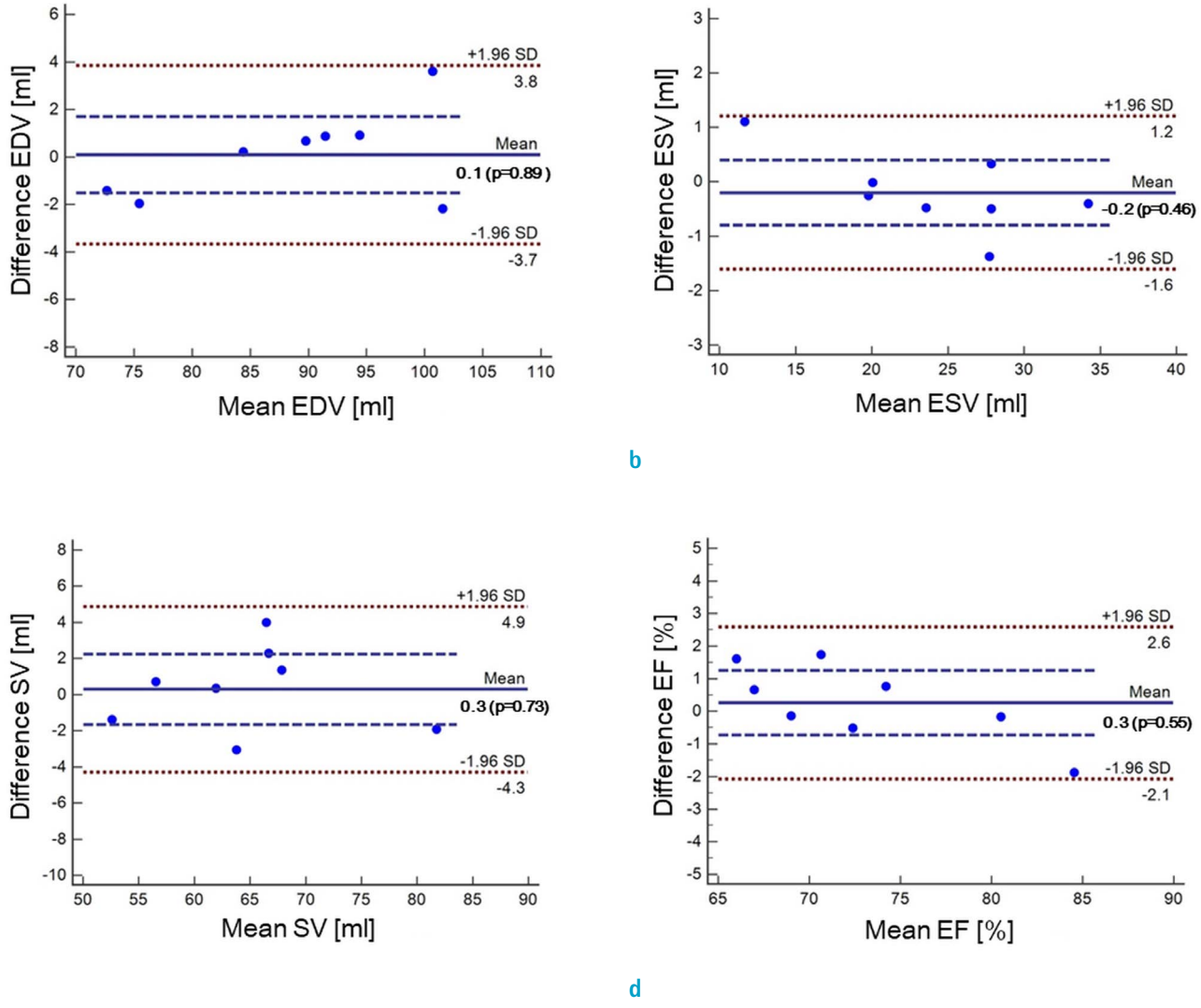

Fig. 6. Bland-Altman plots for assessments of LVF by CS-cine (FOCUSS, CF = 4) and standard cine after compensation: (a) EDV, (b) ESV, (c) SV, and (d) EF. As shown, biases are reduced substantially for all EDV, ESV, SV, and EF.

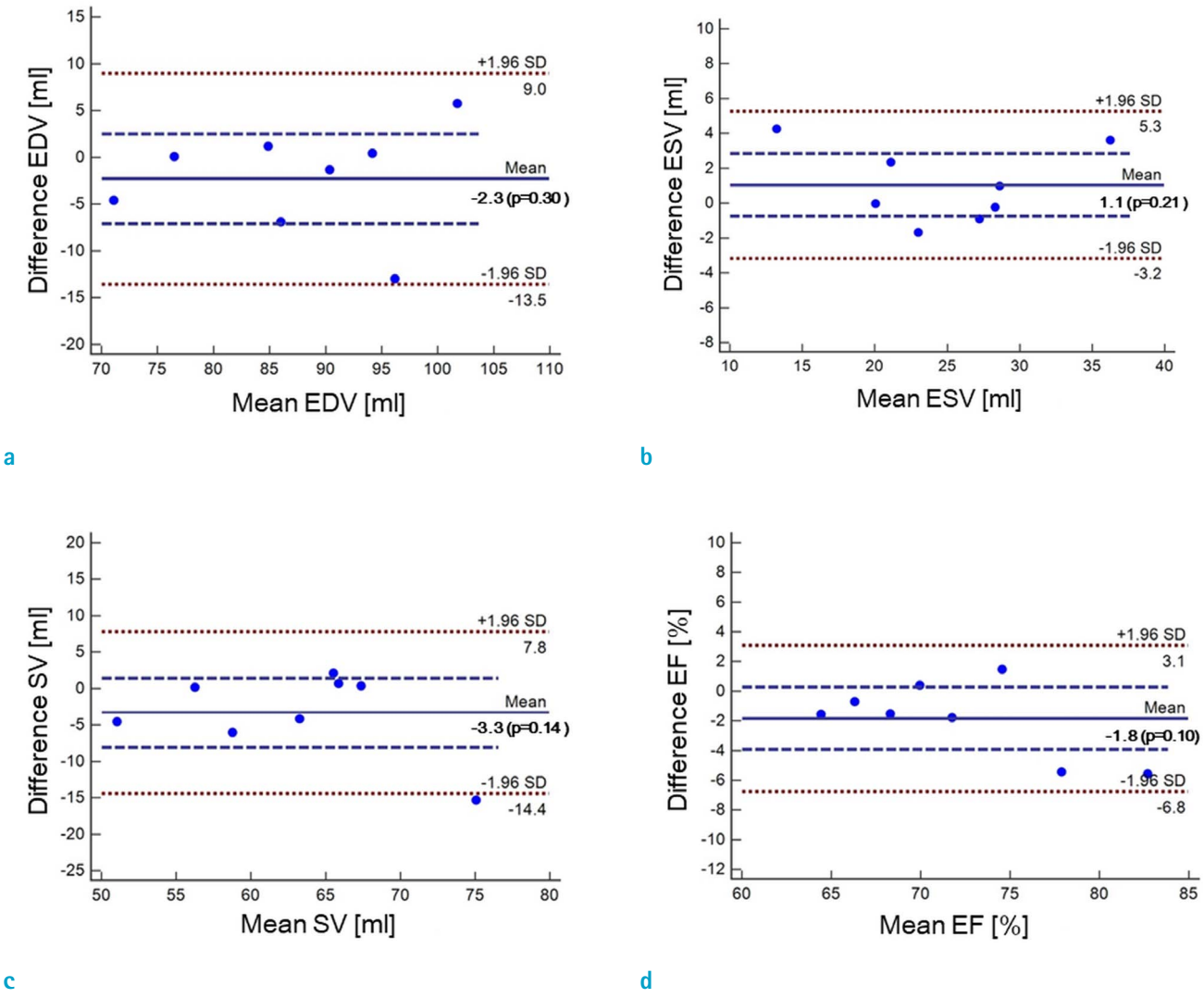

Fig. 7. Bland-Altman plots for assessments of LVF by real-time CS-cine (ITSC, CF = 8) and standard cine after compensation: (a) EDV, (b) ESV, (c) SV, and (d) EF.

under such variations, implying that the biases are larger than the variations. Furthermore, experimental variations would continue decreasing, with improvements of hardware and imaging techniques. Note that compensation removes an average bias, not an individual bias. A more elaborate compensation technique may be developed.

In conclusion, we investigate the error in the assessment of LVF by CS-cine, dominated by bias. The bias is due to a loss of temporal resolution by adopting missing data, from nearby cardiac frames in CS-cine. The bias can be as large as -1.1% to -9.2% for EF with CF from 2 to 8, which can generate a problem in diagnosis. We proposed a simple compensation technique, to reduce the bias with a fixed compensation factor. With compensation, bias is reduced substantially for CS-cine with a retrospective undersampling, as well as with a prospective undersampling (real-time CS-cine). Thus, compensation is useful, in improving assessment of LVF.

Acknowledgments

This work was supported by the National Research Foundation of Korea (NRF) grant funded by the Korean government (MSIT) (No.NRF-2015R1A2A2A03005089, NRF-2019R1A2C2005660). This research has also been conducted through the research grant of Kwangwoon University in 2017.

REFERENCES

1. Lamb HJ, Doornbos J, van der Velde EA, Kruit MC, Reiber JH, de Roos A. Echo planar MRI of the heart on a standard system: validation of measurements of left ventricular function and mass. J Comput Assist Tomogr 1996;20:942-949
2. Epstein FH. MRI of left ventricular function. J Nucl Cardiol 2007;14:729-744
3. Donoho DL. Compressed sensing. IEEE Trans Inf Theory 2006;52:1289-1306
4. Baraniuk RG. Compressive sensing [lecture notes]. IEEE Signal Process Mag 2007;24:118-124
5. Lustig M, Donoho D, Pauly JM. Sparse MRI: The application of compressed sensing for rapid MR imaging. Magn Reson Med 2007;58:1182-1195
6. Candes EJ, Wakin MB. An introduction to compressive sampling. IEEE Signal Process Mag 2008;25:21-30
7. Pruessmann KP, Weiger M, Scheidegger MB, Boesiger P. SENSE: sensitivity encoding for fast MRI. Magn Reson Med 1999;42:952-962
8. Liang D, Liu B, Wang J, Ying L. Accelerating SENSE using compressed sensing. Magn Reson Med 2009;62:1574-1584
9. Otazo R, Kim D, Axel L, Sodickson DK. Combination of compressed sensing and parallel imaging for highly accelerated first-pass cardiac perfusion MRI. Magn Reson Med 2010;64:767-776
10. Feng L, Grimm R, Block KT, et al. Golden-angle radial sparse parallel MRI: combination of compressed sensing, parallel imaging, and golden-angle radial sampling for fast and flexible dynamic volumetric MRI. Magn Reson Med 2014;72:707-717
11. Benkert T, Feng L, Sodickson DK, Chandarana H, Block KT. Free-breathing volumetric fat/water separation by combining radial sampling, compressed sensing, and parallel imaging. Magn Reson Med 2017;78:565-576
12. Park J, Hong HJ, Yang YJ, Ahn CB. Fast cardiac CINE MRI by iterative truncation of small transformed coefficients. Investig Magn Reson Imaging 2015;19:19-30
13. Aurigemma G, Reichek N, Schiebler M, Axel L. Evaluation of aortic regurgitation by cardiac cine magnetic resonance imaging: planar analysis and comparison to Doppler echocardiography. Cardiology 1991;78:340-347
14. Rodevan O, Bjornerheim R, Ljosland M, Maehle J, Smith HJ, Ihlen H. Left atrial volumes assessed by three- and two-dimensional echocardiography compared to MRI estimates. Int J Card Imaging 1999;15:397-410
15. Bak SH, Kim SM, Park S, Kim M, Choe YH. Assessment of left ventricular function with single breath-hold magnetic resonance cine imaging in patients with arrhythmia. Investig Magn Reson Imaging 2017;21:20-27
16. Ngo TA, Lu Z, Carneiro G. Combining deep learning and level set for the automated segmentation of the left ventricle of the heart from cardiac cine magnetic resonance. Med Image Anal 2017;35:159-171
17. White HD, Norris RM, Brown MA, Brandt PW, Whitlock RM, Wild CJ. Left ventricular end-systolic volume as the major determinant of survival after recovery from myocardial infarction. Circulation 1987;76:44-51
18. Lorenz CH, Walker ES, Morgan VL, Klein SS, Graham TP, Jr. Normal human right and left ventricular mass, systolic function, and gender differences by cine magnetic resonance imaging. J Cardiovasc Magn Reson 1999;1:7-21
19. Wu E, Ortiz JT, Tejedor P, et al. Infarct size by contrast enhanced cardiac magnetic resonance is a stronger predictor of outcomes than left ventricular ejection fraction or end-systolic volume index: prospective cohort study. Heart 2008;94:730-736
20. Muthurangu V, Lurz P, Critchely JD, Deanfield JE, Taylor AM, Hansen MS. Real-time assessment of right and left ventricular volumes and function in patients with congenital heart disease by using high spatiotemporal resolution radial k-t SENSE. Radiology 2008;248:782-791
21. Miller S, Simonetti OP, Carr J, Kramer U, Finn JP. MR Imaging of the heart with cine true fast imaging with steady-state precession: influence of spatial and temporal resolutions on left ventricular functional parameters. Radiology 2002;223:263-269
22. Hsiao A, Lustig M, Alley MT, et al. Rapid pediatric cardiac assessment of flow and ventricular volume with compressed sensing parallel imaging volumetric cine phase-contrast MRI. AJR Am J Roentgenol 2012;198:W250-259
23. Goebel J, Nensa F, Schemuth HP, et al. Compressed sensing cine imaging with high spatial or high temporal resolution for analysis of left ventricular function. J Magn Reson Imaging 2016;44:366-374
24. Vincenti G, Monney P, Chaptinel J, et al. Compressed sensing single-breath-hold CMR for fast quantification of LV function, volumes, and mass. JACC Cardiovasc Imaging 2014;7:882-892
25. Bassett EC, Kholmovski EG, Wilson BD, et al. Evaluation of highly accelerated real-time cardiac cine MRI in tachycardia. NMR Biomed 2014;27:175-182
26. Lin ACW, Strugnell W, Riley R, et al. Higher resolution cine imaging with compressed sensing for accelerated clinical left ventricular evaluation. J Magn Reson Imaging 2017;45:1693-1699
27. Kido T, Kido T, Nakamura M, et al. Compressed sensing real-time cine cardiovascular magnetic resonance: accurate assessment of left ventricular function in a single-breath-

hold. J Cardiovasc Magn Reson 2016;18:50
28. Bluemke DA, Boxerman JL, Atalar E, McVeigh ER. Segmented K-space cine breath-hold cardiovascular MR imaging: Part 1. Principles and technique. AJR Am J Roentgenol 1997;169:395-400
29. Scheffler K, Lehnhardt S. Principles and applications of balanced SSFP techniques. Eur Radiol 2003;13:2409-2418
30. Jung H, Sung K, Nayak KS, Kim EY, Ye JC. k-t FOCUSS: a general compressed sensing framework for high resolution dynamic MRI. Magn Reson Med 2009;61:103-116
31. Markl M, Hennig J. Phase contrast MRI with improved temporal resolution by view sharing: k-space related velocity mapping properties. Magn Reson Imaging 2001;19:669-676
32. Lang RM, Bierig M, Devereux RB, et al. Recommendations for chamber quantification: a report from the American Society of Echocardiography's Guidelines and Standards Committee and the Chamber Quantification Writing Group, developed in conjunction with the European Association of Echocardiography, a branch of the European Society of Cardiology. J Am Soc Echocardiogr 2005;18:1440-1463
33. Lang RM, Badano LP, Mor-Avi V, et al. Recommendations for cardiac chamber quantification by echocardiography in adults: an update from the American Society of Echocardiography and the European Association of Cardiovascular Imaging. Eur Heart J Cardiovasc Imaging 2015;16:233-270